Biological and Medical Applications of Materials and Interfaces

Near-field Terahertz Sensing of Hela cells and Pseudomonas Based on Monolithic Integrated Metamaterials with Spintronic Terahertz Emitter

Zhongyang Bai, Yongshan Liu, Ruru Kong, Tianxiao Nie, Yun Sun, Helin Li, Tong Sun, Chandan Pandey, Yining Wang, Haoyi Zhang, Qinglin Song, Guozhen Liu, Michael Kraft, Weisheng Zhao, xiaojun wu, and Lianggong Wen

ACS Appl. Mater. Interfaces, **Just Accepted Manuscript** • DOI: 10.1021/acsami.0c08543 • Publication Date (Web): 09 Jul 2020

Near-field Terahertz Sensing of Hela cells and Pseudomonas Based on Monolithic Integrated Metamaterials with Spintronic Terahertz Emitter.

Zhongyang Bai,[†a,b] Yongshan Liu,[†a,b] Ruru Kong,[a,c] Tianxiao Nie,[a,b] Yun Sun,[a,c] Helin Li,[a,b] Tong Sun,[a,b] Chandan Pandey,[a,b] Yining Wang,[a] Haoyi Zhang,[a] Qinglin Song,[b] Guozhen Liu,[e] Michael Kraft,[f] Weisheng Zhao,[a,b] Xiaojun Wu,*[d,g] Lianggong Wen,*[a,b]*

a. School of Microelectronics, Beihang University, 100191, China.

b. Beihang-Goertek Joint Microelectronics Institute, Qingdao Research Institute of Beihang University, Qingdao, 266000, China. School of Microelectronics, Beihang University, 100191, China.

c. Hefei Innovation Research Institute, Beihang University, Hefei, 230013, China. School of Microelectronics, Beihang University, 100191, China.

d. School of Electronics and Information Engineering, Beihang University, Beijing, 100191, China.

e. Graduate School of Biomedical Engineering, ARC Centre of Excellence in Nanoscale BioPhotonics (CNBP), Faculty of Engineering, University of New South Wales, Sydney, NSW, 2052, Australia.

f. ESAT-MICAS, KU Leuven, Kasteelpark Arenberg 10, 3001 Leuven, Belgium

g. Huazhong University of Science and Technology, Wuhan National Laboratory for Optoelectronics, Wuhan 430074, China

† These authors contributed equally to this work.

TOC Graphic:

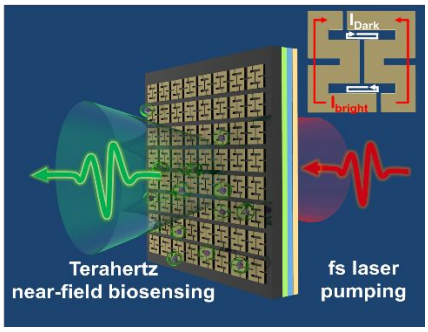

ABSTRACT

Label-free biosensor operating within the terahertz (THz) spectra have helped to unlock a myriad of potential terahertz applications, ranging from bio-material detection to point-of-care (PoC) diagnostics. However, the THz wave diffraction limit and the lack of emitter-integrated THz biosensor are hindering the proliferation of high resolution near-field label-free THz biosensing. Here, a monolithic THz emission biosensor is achieved for the first time by integrating asymmetric double-split ring resonator metamaterials with a ferromagnetic heterojunction spintronic THz emitter. This device exhibits an electromagnetically induced transparency window with resonance frequency of 1.02 THz and a spintronic THz radiation source with a bandwidth of 900 GHz, which are integrated on a fused silica substrate monolithically for the first time. It was observed that the

resonance frequency experienced a redshift behavior along with increasing the concentration of Hela cells and Pseudomonas due to the strong interaction between the spintronic THz radiation and the biological samples on the metamaterials. The spatial frequency redshift resolution is ~ 0.01 THz with a pseudomonas concentration increase from ~ 0.5×10^4/mL to ~ 1×10^4/mL. The monolithic THz biosensor is also sensitive to the sample concentration distribution with 15.68 sensitivity under spatial resolution of 500 μm, which is determined by the infrared pump light diffraction limit. This THz emission biosensor shows great potential for high resolution near-field biosensing applications of trace biological samples.

KEYWORDS

Near-field biosensing, Electromagnetically induced transparency analog, Metamaterials, Spintronic terahertz emitter, Monolithic integration

INTRODUCTION

Label-free terahertz (THz) biosensing offers attractive possibilities for non-invasive detection of malignant cells or other biological samples due to its high sensitivity.[1] Additionally, compared to other electromagnetic waves, THz wave has little side-effects and less heat effect to tissues and biomolecules because of the low photon energy and the non-ionizing effect of THz wave.[2] Label-free THz biosensing techniques can be divided into direct and indirect categories. The direct THz biosensing is achieved by receiving the terahertz signals transmitted from irradiated biological samples,[3] while the indirect THz biosensing is implemented with metamaterials (MM) or metasurfaces.[4,5] Due to the flexibility in the MM or metasurface design, the indirect techniques can be tailored to test a variety of specific target samples, especially for the THz biosensing applications.[6–8]

Several highly sensitive indirect label-free THz biosensing approaches have been reported, including the detection of protein,[9] viruses,[10] and cells.[11] However, these approaches utilize mostly the far-field THz waves, which mainly obtain the macroscopic information of the analyte.[12] Thus, the sensitivity of such technique is limited by the spatial overlap between the analyte and the localized electromagnetic field. Meanwhile, biological samples interacting with near-field THz waves at the source have been previously studied with semiconductor emitters.[13,14] Such technique has demonstrated that emitter-integrated biosensor is an effective solution for near-field THz biosensing. However, semiconductor terahertz emitters based on the terahertz quantum cascade laser (THz-QCL) or photoconductive antenna (PCA) are restricted either by cryogenic conditions or sophisticated III-V fabrication process, making it difficult to facilitate monolithic integrations.[15]

In this paper, a novel THz emission biosensor (TEB) is demonstrated by integrating electromagnetically induced transparency analog (EITA) metamaterials monolithically with a ferromagnetic heterojunction spintronic THz emitter for the first time. EITA with high-Q factor has been widely implemented for THz sensing, due to its high intrinsic sensitivity to the variations of its surrounding dielectric environment.[16,17] The TEB described here utilizes an engineered asymmetric double-split ring resonator array as the EITA metamaterial, processed on the frontside of the fused silica substrate. On the other hand, to exploit appropriate THz emitters for better integration, the recently developed spintronic THz emitter is considered as an alternative THz source for its low cost, large bandwidth, high scalability.[18,19] A layer of W/CoFeB/Pt ultrathin nanofilm has been sputtered onto the backside of the substrate to form the spintronic THz emitter stack. This TEB device allows a highly efficient near-field interaction between the spintronic THz radiation and biological analyte with a potential sub-micron scale spatial resolution.

Cervical cancer cells Hela with green fluorescent proteins (Hela-GFP) and Pseudomonas bacterial sample with blue fluorescence are chosen in the experiments. Firstly, far-field THz biosensing of Pseudomonas and Hela-GFP with different concentrations are tested using photoconductive antenna (PCA) emitter and spintronic THz emitter. In the PCA emitter characterization, the frequency redshifts represent excellent linearity with $R^2 = 0.99$ and $R^2 = 0.92$ for Hela-GFP and Pseudomonas, respectively. The biosensing results have a good consistency in sensing under different sources with *Similarity* of 1.01 and 1.12 for Hela-GFP and Pseudomonas, respectively. Moreover, the results of near-field THz biosensing of Pseudomonas has a maximum frequency redshift of 0.16 THz using TEB, implying a higher sensitivity with 15.68 due to the strong interaction between the spintronic THz radiation and the biological samples on the MM. Such novel THz emission biosensor exhibit promising potential in future near-field biomedical and biological detections.

EXPERIMENTAL SECTION

Design of TEB device. The TEB is combined with a W/CoFeB/Pt trilayer heterostructure and an EITA-MM array for biosensing experiments. The design idea is schematically illustrated in Fig. 1(a). A femtosecond laser beam from a commercial Ti: sapphire laser oscillator is incident onto the surface of the W/CoFeB/Pt THz emitter of which each layer metal thickness is 1.8 nm. THz waves are generated in the heterostructure due to inverse spin Hall effect.[20,21] This THz radiation process is described in Fig. 1 (b). After propagating through a 2.0 mm fused silica substrate, the radiated THz wave directly interacts with the fabricated MM array in near-field scale. Numerous biological samples are adhered to the MM surface for modifying the dielectric environment of the MM, further modulating the emitted THz waves which are recorded by far-field electro-optic sampling detection method in a 1 mm thick ZnTe crystal. Since the diameter of the femtosecond

laser pulse used in the experiment is <1 mm ($1/e^2$) at the THz source, the region of the generated THz beam for near-field biosensing is limited to a small area, only determined by the pumping laser diffraction limit. The MM design parameters are listed in Fig. 1(c), the corresponding structural parameters are p=100 μm, s=88 μm, w=16 μm, h=6 μm, g=4 μm, a=28 μm. The MM structure unit is an asymmetric double-split ring resonator for introducing an EITA Fano resonance, which renders a medium transparency within a narrow spectral range. It is notably mentioned that the structural asymmetric parameter a defined by the displacement of two splits determines the asymmetric degree of MM, which decides the bandwidth of the transparent window. A Scanning Electronic Microscope (SEM) (Zeiss Sigma 300, Germany) photography of a myriad of Pseudomonas adhered onto the surface of MM is shown in Fig.1(d).

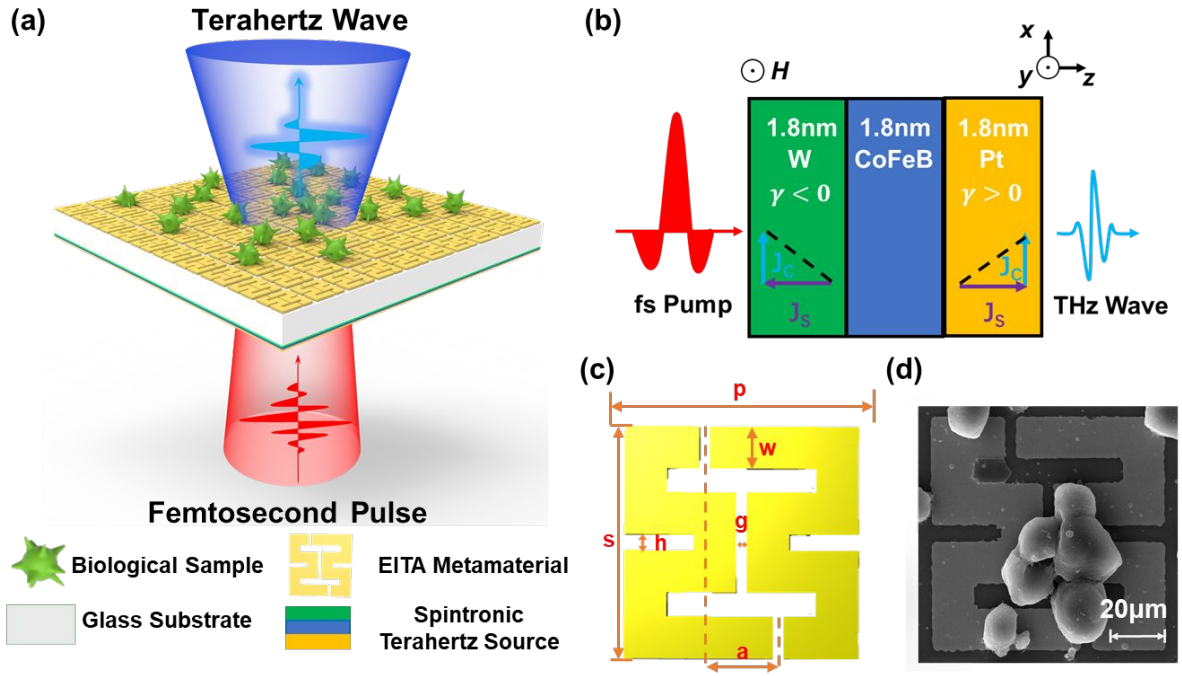

Figure 1. (a) Schematic illustration of the integrated TEB device. The femtosecond laser pulses are incident from the bottom and the radiated terahertz waves pass through the MM, on which biological sample is deployed. (b) The radiation principle of spintronic THz emitter. The spin

current J_s launched by the fs pump excitation is converted into the spin-hall current J_c due to the inverse spin-Hall effect (ISHE). The J_c along the x-axis acts as an electric dipole, emitting THz waves into free space. As W and Pt exhibit the largest spin-Hall angles γ, but with opposite sign, the J_c in W and Pt layer flow the same direction, resulting in the double terahertz output relative to the bilayer film structure. (c) The MM unit parameters of an asymmetric double-split ring resonator (p=100μm, s=88μm, w=16μm, h=6μm, g=4μm, a=28μm). (d) A SEM image showing the Pseudomonas deployed on the surface of the TEB.

Fabrication of the EITA metamaterials. The manufacturing of the MM is exhibited in Fig. 2(a). The substrate was fused silica, which is isotropy and the birefringence was neglected. Two photoresist layers (LOR 5B, MicroChem, Germany; AZ5214E, Clariant GmbH, Germany) were coated onto the substrate using coater (SUSS Spin6, Germany) and heated with 110 °C 100 s on a hotplate (SUSS HP8, Germany). After that, the coated substrates were exposed with the MM pattern using lithography (SUSS MA6, Germany). After development, a 220 nm thickness of Cr/Au films was deposited by an e-beam evaporation (SKY DZS-100, China). Finally, the N-Methyl-2-pyrrolidone (NMP) solvent was used to dissolve residual photoresists, forming the designed MMs.

Culture and preparation of biological samples. Two type biological samples were used in the experiments, including the human cervical cancer cell line Hela with green fluorescence protein (Hela-GFP) and the Pseudomonas with blue fluorescent (Oulu Biotechnology, China). Fig. 2(b) and (c) depict biological samples culture process. For the Hela-GFP cell culture process, the cells were thawed to room temperature first. Thereafter, the cells were placed into a T25 culture flask containing Dulbecco's modified eagle's medium (DMEM) supplemented with 10% fetal bovine

serum (FBS). The flask was stored in an incubator with a temperature of 37 °C and filled with 5% CO2 gas. At the same time, the Pseudomonas was grown in a petri dish for 48 h at 25°C on beef exact peptone AGAR medium (pH=7.0). After biological sample culturing, the biological samples were washed with phosphate buffer saline (PBS) (Solarbio, China) firstly. And then, the samples were centrifuged to remove waste and subsequently resuspended in medium with related concentrations.

Three concentrations of biological samples were measured in this experiment, and the concentration gradient was set to be original concentration (C3, ~1×10^5/mL), 10-fold dilution (C2, ~1×10^4/mL) and 20-fold dilution (C1, ~0.5×10^4/mL) respectively. The sample volume applied onto the chips is 10 μL each time. Each concentration of the biological samples was finally seeded onto a biosensor and air dried at 37 °C for 5 min. Fig. 2(d) shows the bright field and the fluorescent images of the biological samples with three different concentrations and bacterial sample with concentration 1 observed under the microscope (Olympus CKX53).

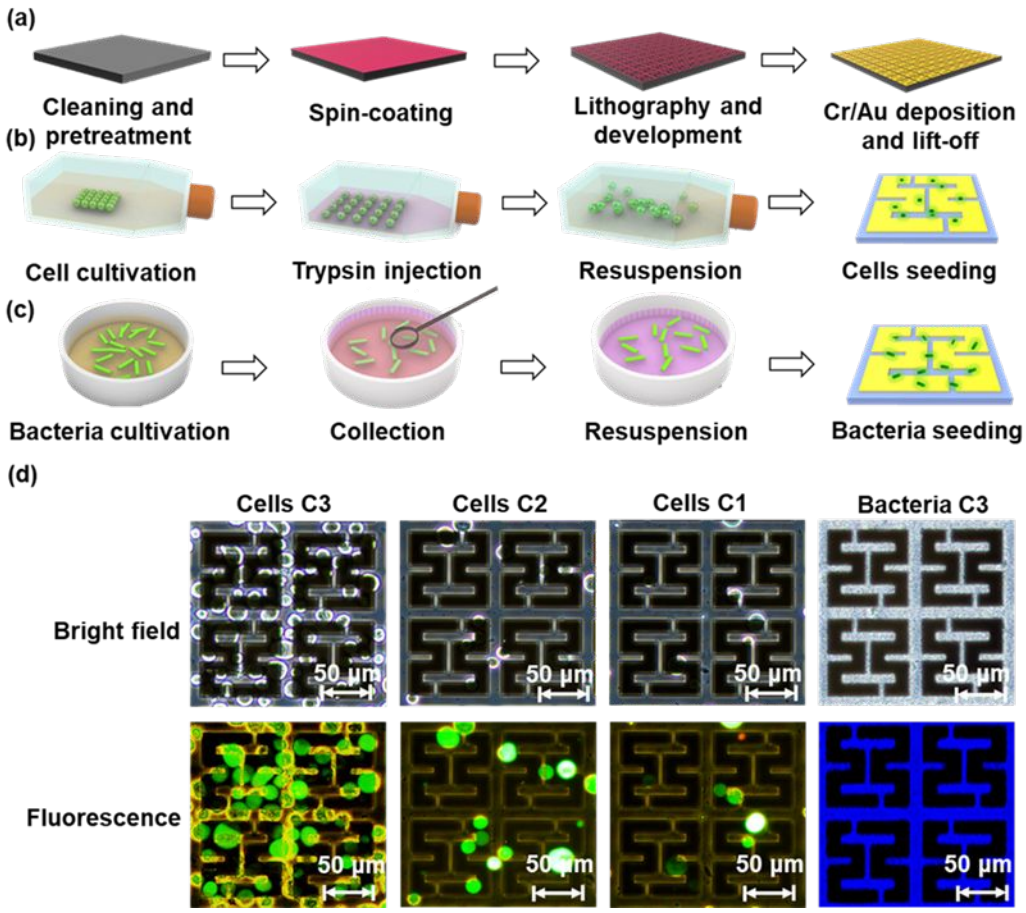

Figure 2. (a) Fabrication process of the TEB. The preprocess of culture and seeding onto the biosensor surface for (b) Hela cells and (c) Pseudomonas, respectively. (d) Bright field and fluorescent photographs of biological sample with different concentrations（C1, C2, C3）on TEB.

Numerical Simulations. In order to study the label-free sensing mechanism of the TEB, the modulated THz emission spectrum response were numerically investigated by the full-wave numerical simulation software integration package (CST Microwave Studio). In this simulation, a cylinder was modeled on the center of MM structure as biological analyte and Occupying Ratio (

OR), which represented the ratio of biological sample area S_{Sample} to a single MM structure was recognized as the variable S_{MM} . The OR definition can be written as:

$$OR = \frac{S_{Sample}}{S_{MM}} \quad (1)$$

The material of biological analyte was set as biological material with permittivity ε=3.67.[22] The THz emission signals of the designed MM were simulated by changing the OR accordingly. As shown in Fig. 3(a), the > 65 % transmission window of single MM is located at 1.0 THz with two peaks which situate at 0.88 THz and 1.16 THz (red line), respectively. Meanwhile, the emission peak redshifted, as the OR being varied from 0 % to 16 %. This indicates that the EITA-MM is highly sensitive to the OR variation of biological samples on the surface. In other words, with the OR increase of the biological sample, the THz emission peak experience a redshift. Furthermore, the corresponding analysis result of the spectral shift at different OR conditions is plotted in Fig. 3(b). From this figure, we can find that the shift frequency and the OR present a positive linear correlation with a maximum variation of Δf = 120.57 GHz at OR =16 %. To further explore the physical characteristic of MM in label-free biosensing, the simulated electromagnetic distribution of MM structure with OR = 2 % at three specific frequencies of f_1 = 0.88 THz, f_2 = 1.0 THz, and f_3 = 1.16 THz was simulated, and the results are summarized in Fig.3 (c)-(h). Their corresponding surface current simulations are illustrated in Fig.3 (c), (e), and (g), respectively. It is shown that incomplete half-cycle currents are formed on both asymmetric sides of the MM structure. On the one hand, the electric dipole resonance mode is generated at f_1 and f_3 , respectively (see Fig. 3(c) and (g)). The factor that contributes to the surface current is a weak magnetic field which is generated on both sides of the asymmetric MM ring as shown in Fig. 3(d) and (h). On the other

hand, there is a complete circulating current in the upper and lower areas of the MM ring structures at f_2, and the response is due to magnetic dipole resonance in Fig. 3(e). A possible explanation is that an external magnetic field in the space surrounded by the MM structure is generated by the circulating current along the electric quadrupole and induces magnetic dipole resonance (Fig. 3(f)). Based on the simulation results, the MM structure forms a quadrupole resonance at f_2. The charge polarity in the MM structure can change at specific frequencies.

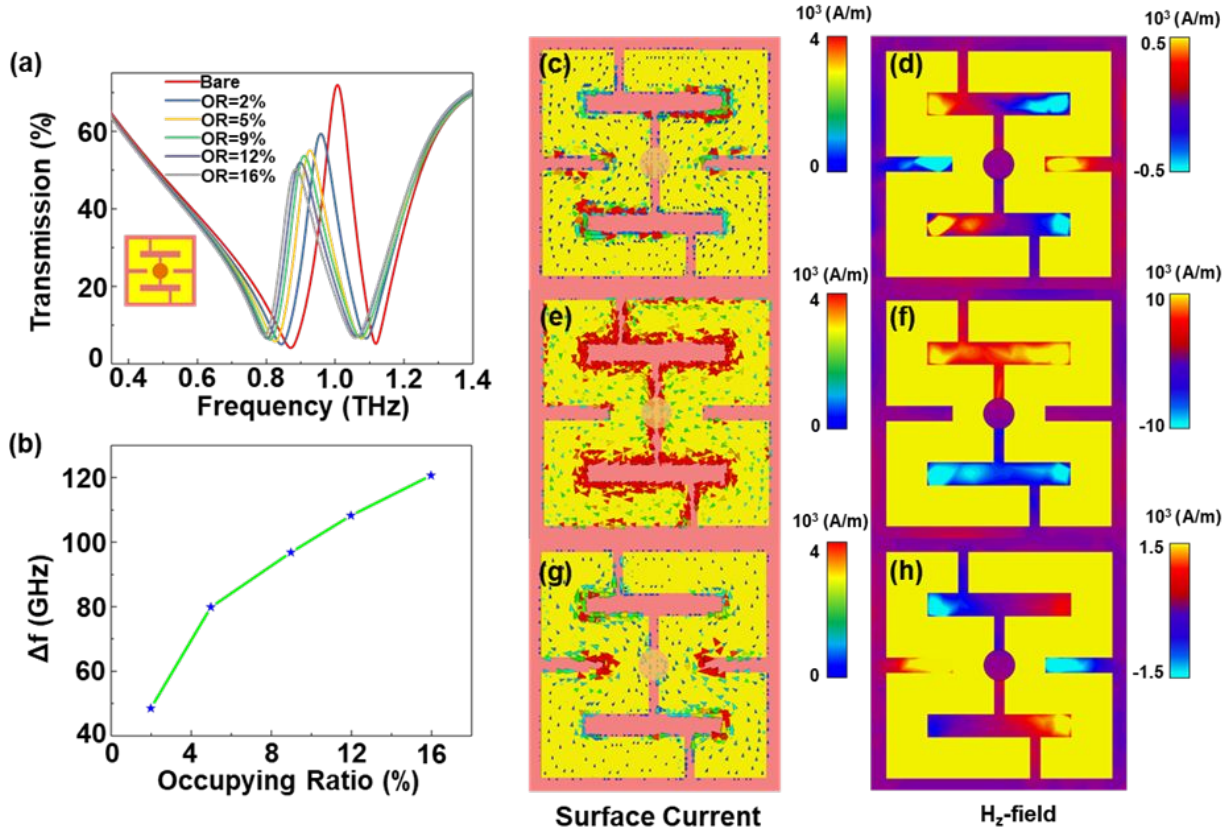

Figure 3. CST simulation results of the designed MM biosensor structure. (a) THz transmission spectra from the MM structure when changing the occupying ratio (OR) of biomaterials in the center of a single MM unit. (b) Corresponding frequency shift at different OR conditions. (c), (e), (g) The surface current simulation diagrams at three different frequency ($f_1 = 0.88$ THz, $f_2 = 1.0$

THz, f_3 = 1.16 THz). (d), (f), (h) The magnetic field in z-axis of MM structure with OR = 2% at relevant frequencies.

Terahertz time domain spectroscopy. The THz emission spectroscopy setup was composed of four parts: a driving laser, an emitter, the optical path, and detection device.[19,23] The driving laser was a commercial Ti: sapphire laser oscillator yielding ultrafast pulses with a central wavelength of 800 nm, pulse duration of 70 fs, and repetition rate of 80 MHz. The femtosecond laser pulses were split into two beams of a generating beam (90 % power) and a detecting beam (10 % power). The generating beam was implemented to pump the TEB and the modulated THz waves were monitored by the electro-optic sampling method in a 1 mm thick ZnTe crystal enabled by the probing beam. In this work, for the TEB characterization, another GaAs photoconductive antenna emitter (Z-omega) were employed to test the samples in a conventional THz time-domain spectrometer with < 5×10^{-9} mbar vacuum to eliminate the water vapor influence.

RESULTS AND DISCUSSION

Far-field biosensing with a GaAs PCA and a spintronic emitter. To corroborate the feasibility of the integrated TEB, label-free biosensing of discrete MM biosensor was performed in a standard home-build THz time-domain spectrometer using both GaAs photoconductive antenna (PCA) and spintronic THz emitters of W/CoFeB/Pt trilayer, respectively. To investigate the THz transmission spectral response of the discrete MM biosensor, the same biological samples used in TEB were measured. As shown in Fig. 4(a), the resonance frequency peaks red shift as the cell concentration increases from C1 (~0.5×10^4 cells/mL) to C2 (~1×10^4 cells/mL) and then to C3 (~1×10^5 cells/mL). Furthermore, as indicated in the star symbol of Fig. 4(e), the frequency variation Δf has a significant change with different cells concentration under GaAs PCA. Δf grows to 0.09 THz under

Cells C1 and changes to 0.15 THz and 0.22 THz with the concentration changes to Cells C2 and Cells C3 respectively. when testing Pseudomonas samples. The resonance frequency peak exhibits a redshift as the increasing concentration gradient of bacteria concentration set up to Bacteria C1, Bacteria C2, and Bacteria C3 (Fig.4(b)). Correspondingly, Δf grows from 0.07 THz under Bacteria C1 and changes to 0.08 THz and 0.13 THz with the concentration changes to Bacteria C2 and Bacteria C3 respectively shown in the positive triangle symbol of Fig. 4(f). By performing a linear fitting analysis on the data of GaAs PCA emitter characterization, the frequency redshifts of biological samples represent an excellent linearity with $R^2 = 0.99$ and $R^2 = 0.92$ for Hela-GFP (the red dotted line of Fig.4(e)) and Pseudomonas (the green dotted line of Fig.4(f)) respectively. The inset picture of Fig.4(e) and (f) presents the SEM image of Hela-GFP cells and Pseudomonas bacteria on the surface of MM biosensor under C3 concentration.

The discrete MM biosensor was also characterized by measuring the transmission ratio with biological samples in the THz-TDS system using spintronic THz emitters of W/CoFeB/Pt trilayer. Fig. 4(c) shows that close to 50% transparent window is located at 1.02 THz with two dips, which situates at 0.88 THz and 1.15 THz for the fabricated MM biosensor. What's more, the resonance frequency peak also redshifts as the cells concentration increases from Cells C1 to Cells C2 and then to Cells C3, which is consistent with the results obtained by changing OR in the simulations. Furthermore, as indicated in the round symbol of Fig. 4(e), the Δf has a significant variation for different cells concentrations. Compared with MM biosensor with no biological samples, Δf grows to 0.08 THz under Cells C1 and changes to 0.16 THz and 0.21 THz with the corresponding concentration changes to Cells C2 and Cells C3, respectively. Besides, the increase of Δf has a strong consistency with the results under spintronic THz emitter with $R^2 = 0.98$ (the yellow solid line of Fig.4(e)). For bacteria measurement, the results of transmission curve are shown in Fig.

4(d). Δf grows from 0.07 THz under Bacteria C1 and changes to 0.10 THz and 0.14 THz with the concentration changes to Bacteria C2 and Bacteria C3, respectively, shown in the inverted triangle symbol of Fig. 4(f). In the orange solid line of Fig. 4(f), the linear fitting of these results shows a better linearity with $R^2 = 0.96$ than the results under GaAs PCA emitter. In the experiments, the similarity of same biomaterial results under spintronic THz emitter and GaAs THz emitter is defined as:

$$Similarity = \frac{Slope_{Spin}}{Slope_{PCA}} \tag{2}$$

where $Slope_{Spin}$ and $Slope_{PCA}$ represent the fitting line slopes of spintronic THz emitter and GaAs THz emitter respectively. The cells sensing results of $Slope_{Spin}$ and $Slope_{PCA}$ is 77.31 and 76.30 separately (Fig. 4(e)), while the results of $Slope_{Spin}$ and $Slope_{PCA}$ is 51.31 and 46.04 for bacterial detection (Fig. 4(f)). The far-field THz biosensing comparison results manifest a good consistency with $Similarity$ of 1.01 and 1.11 for Hela-GFP and Pseudomonas, respectively. This result shows that the biosensor has good consistency in sensing under different sources, at the same time, it can be seen from the difference of fitting line slopes that the measurement results under spintronic THz emitter are more sensitive than the results from GaAs PCA emitter.

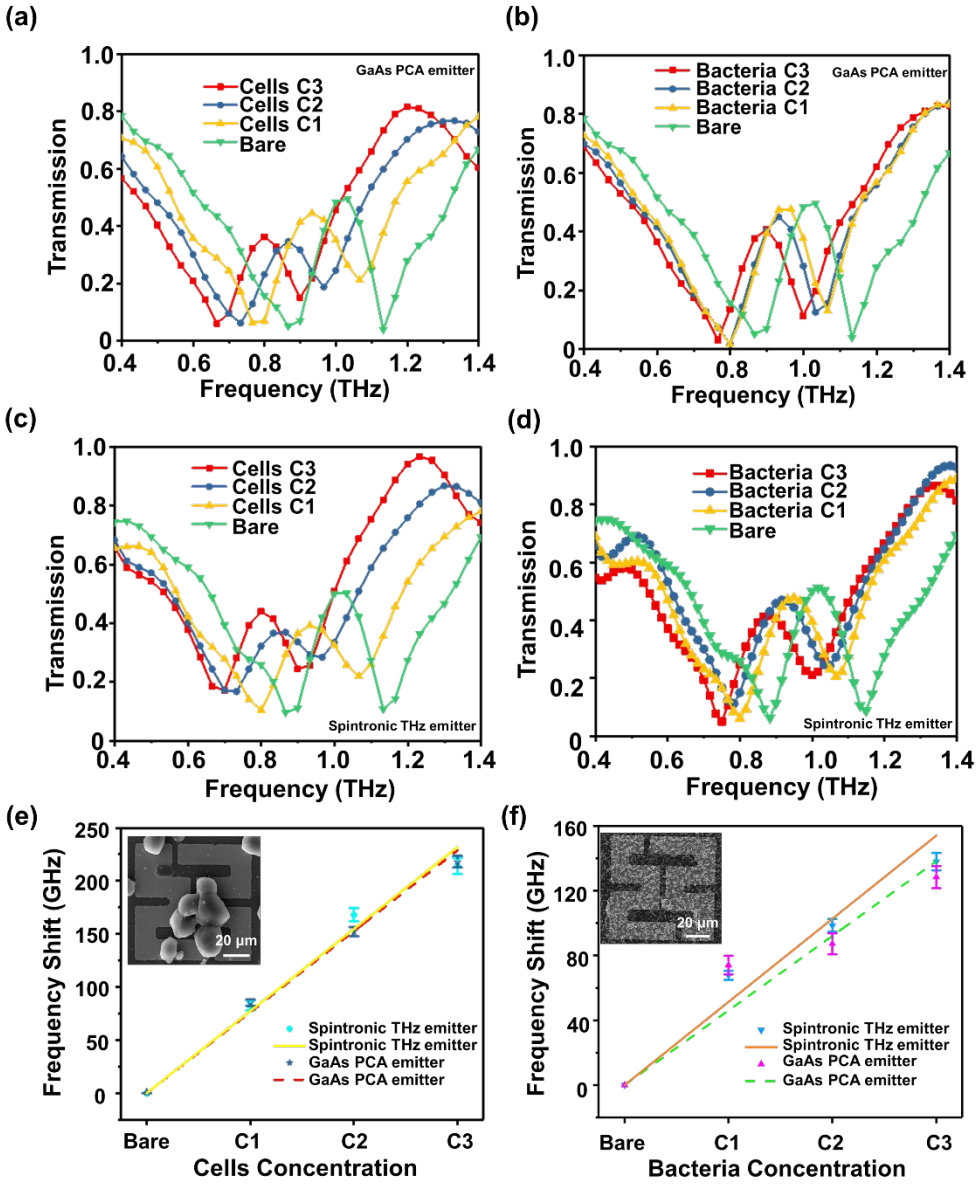

Figure 4. The transmission THz spectra of discrete MM biosensor with biological samples interacting with THz waves from the GaAs PCA emitter (a) (b) and Spintronic THz emitter (c) (d). The EITA transmission window moves to low frequency with different concentrations of Hela cells (a) (c)and of Pseudomonas bacteria (b) (d). The measurement errors of these experiments are analyzed in (e) and (f) (N=5). The frequency shift behaviors as functions of Hela cell (e) and Pseudomonas (f) concentrations, respectively. The insets in (e) and (f) are the SEM images for Hela cells and Pseudomonas on MM surfaces, respectively.

Near-field THz biosensing using TEB. To demonstrate the THz biosensing characteristics of the TEB, the fully integrated device with the bacteria sample were systematically measured in the THz emission spectrometer. The THz emission spectra for various concentrations are shown in Fig. 5(a). When comparing with the device without biomaterials, the THz response of the bacteria-adhesive samples preserved the spectrum shapes and exhibit an EITA resonance frequencies redshift. These responses originate from the variation of the local dielectric environment as discussed in the above-mentioned simulation section. When the sample concentration was increased, the resonance frequency redshifted to 0.95 THz, 0.94 THz and 0.86 THz for the three concentrations, respectively. The fabricated TEB shows the capability of a strong near-field interaction between THz radiation and biological analyte in one device with a maximum frequency response of 0.16 THz, as shown in the inset picture of Fig. 5(a). It indicates that a higher concentration introduces stronger modulation of the local environments, and the experimental results agree very well with the theoretical predictions.

For the integrated TEB, spin current is only generated at the femtosecond laser irradiation position in the W/CoFeB/Pt heterostructure, which is closely related to the THz radiation area. This leads to the fact that only the MM units of the integrated sensor covered by the THz irradiation can be activated and be monitored. Therefore, the effective area of the THz biosensor is only limited by the femtosecond laser irradiation area, implying a much higher spatial resolution for trace detection applications. In Fig. 5(b), two different positions were selected on one TEB device, which was coated with the same bacteria sample for the THz emission measurement. The results show a 0.02 THz frequency variation of the two measurement positions, which can be attributed to the inhomogeneous distribution of the biological sample on the MM surface. To rule out the heat effect introduced by femtosecond laser illumination onto the biomaterials, we repeated the

measurements for a time interval of 10 minutes and obtain consistent experimental results as that from short time THz radiation. These results demonstrate that TEB has the ability to spatially resolve the non-uniformity of concentration distribution of biological samples, which has potential significance in small scale near-field THz biosensing detection.

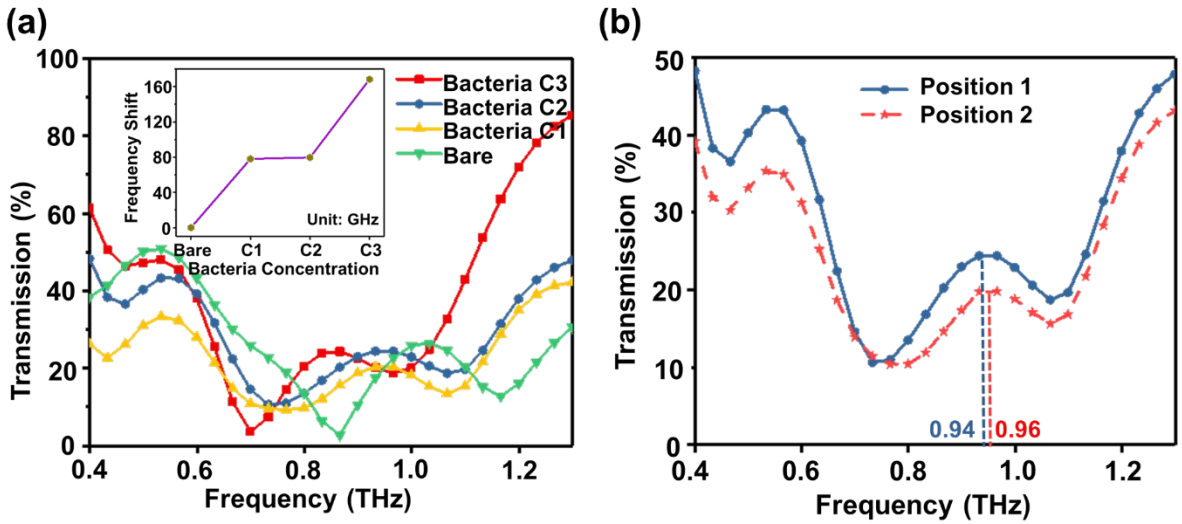

Figure 5. (a) THz transmission spectra of different bacteria concentrations (Bacteria C1, C2, C3) obtained with the TEB. The inset curve shows the values of frequency shifts with different concentrations. (b) For different positions on the same TEB device with the bacteria concentration C2, the THz emission spectra manifest differential behavior with a frequency redshift Δf = 13 GHz and a 4.6 % transmission amplitude variation, showing TEB has the ability to spatially resolve the non-uniformity of the surface biological sample concentration.

Table 1 summarizes the biosensing performance comparison between the fully integrated TEB, Discrete spintronic THz emitter and Discrete GaAs antenna emitter with the Pseudomonas biological samples. It is clear that the fully integrated device exhibits high frequency response to concentration variations with a maximum frequency redshift of 0.16 THz under Bacteria C3. At the same time, due to the near-field interaction of biological samples and terahertz waves, TEB

has the highest sensitivity of 15.68 compared to other devices (Supporting Material Table S1).

Table 1. Summary of the performances of EITA metamaterials with discrete spintronic THz emitter or discrete GaAs PCA and integrated TEB.

	TEB	Discrete spintronic THz emitter	Discrete GaAs PCA emitter
Δf for C1	0.07 THz	0.07 THz	0.07 THz
Δf for C2	0.08 THz	0.10 THz	0.08 THz
Δf for C3	0.16 THz	0.14 THz	0.13 THz
Spatial resolution	~500 μm	~3 mm	~3 mm
Number of effective MM units	~25	~900	~900
Concentration ratio	Low	High	High

CONCLUSION

In conclusion, a novel terahertz emission biosensor based on the monolithic integration of a spintronic terahertz emitter with EITA metamaterials have been firstly demonstrated for near-field biosensing application. Comparison studies employing Hela cells and Pseudomonas with different concentrations have been conducted to benchmark the proposed integrated device. Discrete device schemes were initially compared, and frequency redshift behaviors are observed in both GaAs PCA and spintronic emitter scenarios, which agrees well with the Multiphysics numerical analysis. The designed MM perform excellent frequency response linearity of $R^2 = 0.99$ and $R^2 = 0.92$ for Hela-GFP and Pseudomonas respectively with the GaAs PCA emitter. With the spintronic THz emitter, the frequency response linearity fitting slope is similar to the GaAs PCA emitter scenario

with the *Similarity* of 1.01 for Hela-GFP, and 1.11 for Pseudomonas. Eventually, the fully integrated TEB shows a strong near-field interaction between the THz radiation and the biological analyte with a maximum frequency redshift of 0.16 THz and *Sensitivity* of 15.68. The metamaterial design and the spintronic nanofilms stacks can be further optimized according to specific applications. Owing to the compact integration of the spintronic THz emitter with the metamaterials, the proposed TEB has superior characteristics as a promising low-cost near-field THz biosensor option with high sensitivity under small-scale spatial resolution.

ASSOCIATED CONTENT

Supporting Information

The comparison of structural and sensitivity performance of other purposed biosensors and this work.

AUTHOR INFORMATION

Corresponding Author

* E-mail:

Lianggong Wen Email: wenlg@bhqditi.com

Xiaojun Wu Email: xiaojunwu@buaa.edu.cn

Tianxiao Nie Email: nietianxiao@buaa.edu.cn

Author Contributions

The manuscript was written through contributions of all authors. All authors have given approval to the final version of the manuscript.

Notes

The authors declare no competing financial interest.

ACKNOWLEDGMENT

This work is supported by the National Key R&D Program of China (No. 2018YFB0407602), National Natural Science Foundation of China (61774013, 11827807, 61905007, 4194083), the International Collaboration Project (B16001), the National Key Technology Program of China (2017ZX01032101), the Open Project Program of Wuhan National Laboratory for Optoelectronics (NO.2018WNLOKF001). This study is also supported by the "Zhuoyue Program" of Beihang University (ZG216S18B5), Qingdao Innovation and Entrepreneurship Leadership Program (18-1-2-21-zhc), and the VR innovation platform from Qingdao Science and Technology Commission and Magnetic Sensor innovation platform from LaoShan District. G.Liu acknowleges the Australian Research Council Future Fellowship (FT160100039).

ABBREVIATIONS

TEB, terahertz emission biosensor; MM, metamaterials; EITA, electromagnetically induced transparency analog; ISHE, inverse spin-Hall effect; PCA, photoconductive antenna

REFERENCES

(1) Ahmadivand, A.; Gerislioglu, B.; Ahuja, R.; Mishra, Y. K. Terahertz Plasmonics: The Rise of Toroidal Metadevices towards Immunobiosensings. *Mater. Today* **2019**.

(2) Xu, W.; Xie, L.; Ying, Y. Mechanisms and Applications of Terahertz Metamaterial Sensing: A Review. *Nanoscale* **2017**, *9* (37), 13864–13878. https://doi.org/10.1039/c7nr03824k.

(3) Wu, X.; Yiwen, E.; Xu, X.; Wang, L. Label-Free Monitoring of Interaction between DNA and Oxaliplatin in Aqueous Solution by Terahertz Spectroscopy. *Appl. Phys. Lett.* **2012**, *101* (3), 3–7. https://doi.org/10.1063/1.4737401.

(4) O'Hara, J. F.; Singh, R.; Brener, I.; Smirnova, E.; Han, J.; Taylor, A. J.; Zhang, W. Thin-Film Sensing with Planar Terahertz Metamaterials: Sensitivity and Limitations. *Opt. Express* **2008**, *16* (3), 1786. https://doi.org/10.1364/oe.16.001786.

(5) Withayachumnankul, W.; Lin, H.; Serita, K.; Shah, C. M.; Sriram, S.; Bhaskaran, M.; Tonouchi, M.; Fumeaux, C.; Abbott, D. Sub-Diffraction Thin-Film Sensing with Planar Terahertz Metamaterials. *Opt. Express* **2012**, *20* (3), 3345–3352.

(6) Gupta, M.; Singh, R. Terahertz Sensing with Optimized Q/Veff Metasurface Cavities. *Adv. Opt. Mater.* **2020**, *1902025*, 1–7. https://doi.org/10.1002/adom.201902025.

(7) Zhang, Z.; Yang, M.; Yan, X.; Guo, X.; Li, J.; Yang, Y.; Wei, D.; Liu, L.; Xie, J.; Liu, Y. The Antibody-Free Recognition of Cancer Cells Using Plasmonic Biosensor Platforms with the Anisotropic Resonant Metasurfaces. *ACS Appl. Mater. Interfaces* **2020**.

(8) Srivastava, Y. K.; Ako, R. T.; Gupta, M.; Bhaskaran, M.; Sriram, S.; Singh, R. Terahertz Sensing of 7 Nm Dielectric Film with Bound States in the Continuum Metasurfaces. *Appl. Phys. Lett.* **2019**, *115* (15). https://doi.org/10.1063/1.5110383.

(9) Wu, X.; Quan, B.; Pan, X.; Xu, X.; Lu, X.; Gu, C.; Wang, L. Alkanethiol-Functionalized Terahertz Metamaterial as Label-Free, Highly-Sensitive and Specific Biosensor. *Biosens Bioelectron* **2013**, *42*, 626–631. https://doi.org/10.1016/j.bios.2012.10.095.

(10) Park, S. J.; Cha, S. H.; Shin, G. A.; Ahn, Y. H. Sensing Viruses Using Terahertz Nano-Gap Metamaterials. *Biomed. Opt. Express* **2017**, *8* (8), 3551. https://doi.org/10.1364/boe.8.003551.

(11) Zhang, Z.; Ding, H.; Yan, X.; Liang, L.; Wei, D.; Wang, M.; Yang, Q.; Yao, J. Sensitive Detection of Cancer Cell Apoptosis Based on the Non-Bianisotropic Metamaterials Biosensors in Terahertz Frequency. *Opt. Mater. Express* **2018**, *8* (3), 659–667.

(12) Serita, K.; Murakami, H.; Kawayama, I.; Tonouchi, M. A Terahertz-Microfluidic Chip with a Few Arrays of Asymmetric Meta-Atoms for the Ultra-Trace Sensing of Solutions. *Photonics* **2019**, *6* (1). https://doi.org/10.3390/photonics6010012.

(15) Burford, N. M.; El-Shenawee, M. O. Review of Terahertz Photoconductive Antenna Technology. *Opt. Eng.* **2017**, *56* (1), 010901. https://doi.org/10.1117/1.oe.56.1.010901.

(16) Ding, C.; Jiang, L.; Wu, L.; Gao, R.; Xu, D.; Zhang, G.; Yao, J. Dual-Band Ultrasensitive THz Sensing Utilizing High Quality Fano and Quadrupole Resonances in Metamaterials. *Opt. Commun.* **2015**, *350*, 103–107.

(17) Yan, X.; Yang, M.; Zhang, Z.; Liang, L.; Wei, D.; Wang, M.; Zhang, M.; Wang, T.; Liu, L.; Xie, J. The Terahertz Electromagnetically Induced Transparency-like Metamaterials for Sensitive Biosensors in the Detection of Cancer Cells. *Biosens. Bioelectron.* **2019**, *126*, 485–492.

(18) Seifert, T.; Jaiswal, S.; Martens, U.; Hannegan, J.; Braun, L.; Maldonado, P.; Freimuth, F.; Kronenberg, A.; Henrizi, J.; Radu, I. Efficient Metallic Spintronic Emitters of Ultrabroadband Terahertz Radiation. *Nat. Photonics* **2016**, *10* (7), 483.

(19) Kong, D.; Wu, X.; Wang, B.; Nie, T.; Xiao, M.; Pandey, C.; Gao, Y.; Wen, L.; Zhao, W.; Ruan, C. Broadband Spintronic Terahertz Emitter with Magnetic-Field Manipulated Polarizations. *Adv. Opt. Mater.* **2019**.

(20) Kampfrath, T.; Battiato, M.; Maldonado, P.; Eilers, G.; Nötzold, J.; Mährlein, S.; Zbarsky, V.; Freimuth, F.; Mokrousov, Y.; Blügel, S. Terahertz Spin Current Pulses Controlled by Magnetic Heterostructures. *Nat. Nanotechnol.* **2013**, *8* (4), 256.

(21) Wade, C. G.; Šibalić, N.; de Melo, N. R.; Kondo, J. M.; Adams, C. S.; Weatherill, K. J. Real-Time near-Field Terahertz Imaging with Atomic Optical Fluorescence. *Nat. Photonics* **2017**, *11* (1), 40.

(22) Gabriel, C. *Compilation of the Dielectric Properties of Body Tissues at RF and Microwave Frequencies.*; King's coll london (United Kingdom) dept of physics, 1996.

(23) Chen, X.; Wu, X.; Shan, S.; Guo, F.; Kong, D.; Wang, C.; Nie, T.; Pandey, C.; Wen, L.; Zhao, W. Generation and Manipulation of Chiral Broadband Terahertz Waves from Cascade Spintronic Terahertz Emitters. *Appl. Phys. Lett.* **2019**, *115* (22), 221104.